The Paleochrono-1.1 probabilistic model to derive optimized and consistent chronologies for several paleoclimatic sites

Frédéric Parrenin[1], Marie Bouchet[2], Christo Buizert[3], Emilie Capron[1], Ellen Corrick[4], Russell Drysdale[5], Kenji Kawamura[6], Amaëlle Landais[2], Robert Mulvaney[7], Ikumi Oyabu[6], Sune Rasmussen[8]

5   [1]Univ. Grenoble Alpes, CNRS, INRAE, IRD, Grenoble INP, IGE, 38000 Grenoble, France
[2]UMR8212, CEA–CNRS–UVSQ–UPS, Laboratoire des Sciences du Climat et de l'Environnement (IPSL), Gif-sur-Yvette, France
[3]College of Earth, Ocean and Atmospheric Sciences, Oregon State University (OSU), Corvallis, OR, USA
[4]School of Earth, Atmosphere and Environment, Monash University, Clayton, Victoria, Australia
10   [5]School of Geography, The University of Melbourne, Melbourne,Victoria, Australia.
[6]National Institute of Polar Research, Research Organizations of Information and Systems, 10-3 Midori-cho, Tachikawa, Tokyo 190-8518, Japan
[7]British Antarctic Survey, Madingley Road, High Cross, Cambridge, CB3 0ET, UK
[8]Physics of Ice, Climate and Earth, Niels Bohr Institute, University of Copenhagen, Copenhagen,
15   Denmark.

Correspondence to: Frédéric Parrenin (frederic.parrenin@univ-grenoble-alpes.fr)

Abstract Past climate and environmental changes can be reconstructed using paleoclimate archives such as ice cores, lake and marine sediment cores, speleothems, tree rings and corals. The dating of these natural archives is crucial for deciphering the temporal sequence of events and rates of change during past

20   climate changes. It is also essential to provide quantified estimates of the absolute and relative errors associated with the inferred chronologies. However, this task is complex since it involves combining different dating approaches at different paleoclimatic sites and often on different types of archives. Here we present *Paleochrono-1.1*, a new probabilistic model to derive a common and optimised chronology for several paleoclimatic sites with potentially different types of archives. Paleochrono-1.1 is based on

25   the inversion of an archiving model: a varying deposition rate (also named growth rate, sedimentation rate or accumulation rate) and also, for ice cores, a lock-in-depth of air (since, in the absence of significant surface melt, the air is trapped in the ice at about 50-120 m below the surface) and a thinning function (since glacier ice undergoes flow). Paleochrono-1.1 integrates several types of chronological information: prior knowledge of the archiving process, independently dated horizons, depth intervals of known

30   duration, undated stratigraphic links between records, and, for ice cores, Δdepth observations (depth

differences between events recorded synchronously in the gas and solid phases of a certain core). The optimization is formulated as a least-squares problem, assuming that all probability densities are near-Gaussian and that the model is nearly linear in the vicinity of the best solution. Paleochrono-1.1 is the successor of IceChrono, which produces common and optimized chronologies for ice-cores. Paleochrono-1.1 outperforms IceChrono in terms of computational efficiency, ease of use, and accuracy. We demonstrate the ability of Paleochrono-1.1 in a new ice-core–speleothem dating experiment, which combines the Antarctic Ice Core Chronology 2023 dating experiment, based on records from five polar ice cores, with data from two speleothems dated using uranium/thorium radiometric techniques from Hulu Cave (China). We analyse the performance of Paleochrono-1.1 in terms of computing time and memory usage in various dating experiments. Paleochrono-1.1 is freely available under the MIT open-source license.

1 Introduction

Numerous natural archives provide records of the past evolution of climate and environment. Continuous paleoclimate archives require a continuous deposition process. Examples are: ice cores (e.g., NorthGRIP project members, 2004; EPICA community members et al., 2004; EPICA Community Members et al., 2006; NEEM community Members, 2013; WAIS Divide Project Members, 2013; Dome Fuji Ice Core Project Members et al., 2017), marine sediment cores (e.g., Lisiecki and Raymo, 2005; Elderfield et al., 2012; Shackleton, 2000; Shackleton et al., 2000), lake sediment cores (e.g., Williams et al., 1997; Hodell et al., 1999) and speleothems (e.g., Wang et al., 2001; Cheng et al., 2018; Corrick et al., 2020). Such archives can directly record or more indirectly reflect various climatic parameters, such as local atmospheric or oceanic temperature, precipitation amount and seasonality, sedimentation or precipitation rate, atmospheric composition, sea level, ocean circulation intensity, insolation or biosphere activity.

For paleoclimate archives to provide precise insight into past climate change, it is a prerequisite to be able to derive the age of the archive at each depth level, i.e. to derive an associated chronology. This is, however, a complex task which involves different dating methods (Brauer et al., 2014), depending on the

archive type and the temporal coverage. We will not go into the detail of each method for every archive, but we list here the different types of chronological information:

1) **Modelling of the archiving process:** it is often possible to model deposition through time. For an ice core, this is complicated by the fact that air bubbles are trapped at depth and not at the surface, hence the air is systematically younger than the surrounding ice by a non-constant amount. Moreover, ice layers thin with time due to ice flow. For some archives, the sedimentation or growth rate may vary abruptly due to climatic or local environmental factors, making it a challenge to accurately describe the deposition/growth.

2) **Dated horizons:** some horizons in the archive can be dated using an independent method. Examples include a volcanic ash layer that is dated either from historical records or by radiometric dating of the ash, a paleomagnetic or solar event identified by variations in the ^{10}Be concentration or remanent magnetization, or an event dated by radiometric analysis such as U/Th, ^{14}C or ^{81}Kr.

3) **Intervals of known duration:** sometimes, a section of an archive is of known duration (typically, a section where annual layers can be counted), although the absolute age of the section may not be known accurately.

4) **Stratigraphic links:** links can be derived between the depths of several paleoclimate sites that are known (or assumed) to have the same age. Typically, this can be the same volcanic event recognized at different sites, or an abrupt Dansgaard-Oeschger event seen in multiple proxy records which is assumed to be synchronously recorded within a given margin.

5) $\Delta_{\mathbf{depth}}$ **observations:** can be seen as stratigraphic links between ice and air phases of a single ice-core site (Parrenin et al., 2012).

Each dating method and paleoclimate archive has strengths and weaknesses in terms of chronological construction. For example, ice cores have robust archiving models, which accurately describe the processes of snow deposition, densification and ice flow (e.g., Parrenin et al., 2004, 2007) and at some sites, the annual layers can be counted over long sections (e.g., Sigl et al., 2016; Svensson et al., 2008). However, ice cores generally do not have strong constraints on absolute ages beyond the last millenia. Speleothems can be dated very accurately and precisely using uranium-thorium (U-Th) dating methods (e.g., Cheng et al., 2018). However, speleothem records are often less continuous than ice or marine

sediment records due to hiatuses in calcite precipitation, which can be related to drier or colder conditions
above the cave but may also be unrelated to climate (e.g. due to changes in the percolation path of the
source waters). Marine sediment cores have the longest temporal extent (e.g., Lisiecki and Raymo, 2005).
However, prior to the radiocarbon dating limit (~50 kyr BP, thousands of years before 1950 A.D.), their
chronologies rely on tuning to different reference records such as those based on the calculation of Earth's
orbital parameters (Laskar et al., 2004). In palaeoclimatology, it is typical to treat individual records
independently, making difficult the comparisons between chronologies. Combining chronological data
from multiple archives, across various archive types, has the potential to improve our chronological
framework. An appropriate strategy is to combine the results from the different dating methods and
paleoclimatic sites using a probabilistic framework in order to make the best out of the different archives
and records.

A probabilistic framework was originally developed for polar ice cores using the Bayesian model *Datice*
(Lemieux-Dudon et al., 2010b, 2015). Datice produces an optimal chronology using different types of
chronological information from multiple ice cores. Using this method, the ice-core chronology is derived
from an archiving model that relies on the three canonical glaciological quantities of the ice-core dating
problem: the deposition rate also called accumulation rate, the lock-In depth (LID) of air and the thinning
function,(i.e. ratio of the present-day thickness of an annual layer to its initial thickness when it was
deposited at the surface. In Bayesian terminology, the initial estimate of this archive model is called the
prior scenario.

Datice then seeks an optimal scenario, which is the best compromise between the prior scenario of the
archiving process and the various chronological data. Datice was used in the construction of the reference
chronology Antarctic Ice Core Chronology 2012 (hereafter AICC2012), combining archiving models and
chronological information from four Antarctic and one Greenland ice cores (Bazin et al., 2013; Veres et
al., 2013). Datice was entirely coded in Fortran and, although a powerful tool in terms of performance,
was difficult to use and to modify.

The *IceChrono* dating model (Parrenin et al., 2015) was developed, based on the same principles as
Datice, providing improvements and simplifications in the mathematical, numerical and programming
aspects with respect to Datice. However, IceChrono is sometimes slower than Datice depending on the

resolution chosen, in particular because IceChrono performs a numerical gradient calculation while Datice has a more efficient analytical gradient calculation. IceChrono is coded in Python 2.

Both Datice and IceChrono were initially developed for ice core studies. Technically, it is possible to use these dating tools to combine chronological information from other paleoclimatic archives by fixing the thinning function at unity and by discarding the air bubbles variable (Bazin et al., 2019), but the models are not designed for this purpose.

In this paper, we present a new probabilistic model, named *Paleochrono-1.1*, which is the successor of IceChrono. Paleochrono-1.1 is specifically designed to combine chronological information from multiple types of archives. Paleochrono-1.1 is coded in Python 3 and is more efficient, easier to use and more accurate than IceChrono. We first detail the Paleochrono-1.1 methodology (section 2) and demonstrate its utility with a dating experiment that combines ice cores and speleothems (section 3). We then present the computing resources used by Paleochrono-1.1 in various dating experiments (section 4) and discuss our results (section 5).

2 Method

Paleochrono-1.1 is designed to work with paleoclimatic archives where it can be assumed that the deposition rate is strictly positive at any time. Paleochrono-1.1 does not integrate information regarding hiatuses, working at a temporal resolution where this assumption is valid (because, for example, it does not snow everyday on an ice sheet). We use the term *site*, to refer to one individual archive; we do not use the term record since it can mean a particular proxy within a site. We use *depth* in a broader sense to refer to the distance along the archive, from the youngest to the oldest section. The age along the archive is therefore continuous and strictly increasing. If there is a known hiatus in the archive, the sections before and after the hiatus should be considered as two different sites in Paleochrono-1.1.

Paleochrono-1.1 is set up for two types of archives: the so-called *simple archives*, with one unique depth-age relationship, constant density, and no post-depositional thinning (e.g., speleothems, marine sediments), and *ice-core archives*, where we deal with two ages (one for the ice matrix and one for the enclosed air), variable density, and where post-depositional thinning occurs.

2.1 Method summary

The true chronology of a paleoclimate site is a function of the deposition rate. In the case of ice cores,
140 two additional variables must also be considered: the LID of the air bubbles and the thinning function.
These variables form what we call the forward model, and they are unknown. To find the optimal
chronology, they must be estimated based on:

• Prior information about their values at each site;

• Chronological observations (Figure 1) such as: ages at certain depths, the time elapsed between two
145 depths, the synchronicity of events recorded at two different sites that are assumed capable of recording
events simultaneously, or the depth difference of air and ice levels of the same age within the same ice
core (Δ_{depth}).

All these different types of information, which can be mathematically described as probability density
functions (PDF), are assumed to be independent and are combined together using a Bayesian framework
150 to obtain posterior estimates of the input variables (deposition rate and, for an ice core, LID, and thinning)
and of the resulting chronologies. Uncertainties on the prior estimates and on the observations are
assumed to be Gaussian and the forward model is linearized, allowing this problem to be solved as a least-
square optimization.

2.2 The forward model

2.2.1 For a simple archive

For a simple archive, the archiving model is:

$$\chi(z) = \chi_0 + \int_{z_0}^{z} \frac{dz'}{a(z')} \tag{1}$$

where z is the depth along the paleoclimatic record, $\chi(z)$ is the age at depth z, χ_0 is the age at the top
depth $z = z_0$ (i.e. the age of the youngest material at the site), and a is the depth-dependent deposition
rate at the site of deposition.

160 This equation integrates along the depth axis the number of annual layers per unit depth from the surface.

2.2.2 For an ice-core archive

For an ice-core site, the archiving model is slightly more complicated, since we need to account for the age of the air inside the ice and for the vertical thinning of ice layers:

$$\chi(z) = \chi_0 + \int_{z_0}^{z} \frac{D(z')}{a(z')\tau(z')} \, dz', \tag{2}$$

$$\psi(z) = \chi(z - \Delta_{\text{depth}}(z)), \tag{3}$$

$$\int_{z-\Delta_{\text{depth}}(z)}^{z} \frac{D(z')}{\tau(z')} \, dz' = l(z) \times \left. \frac{D}{\tau} \right|_{firn}^{0}, \tag{4}$$

where z is the depth along the ice core, $\chi(z)$ is the age of the ice at depth z, χ_0 is the age of the ice at the top (with depth $z = z_0$), a is the deposition rate along the ice core, D is the (dimensionless) relative density of the snow/ice material, τ is the vertical thinning function (also dimensionless), ψ is the age of the air, Δ_{depth} is the depth difference between air and ice of the same age, l is the lock-in-depth of air bubbles and $\left. \frac{D}{\tau} \right|_{firn}^{0}$ is the average value of $\frac{D}{\tau}$ in the firn when the air particle was at the lock-in-depth (this parameter is usually ~0.7 for most firns, see Parrenin et al., 2012).

Equation 2 integrates along the depth axis the number of annual layers per unit depth from the surface. Equation 3 describes that the air age at depth z is equal to the ice age at depth $z - \Delta_{\text{depth}}$, which is the definition of Δ_{depth}. Equation 4 describes that if one corrects a depth interval between an ice depth and the depth of air of the same age for thinning, one gets the initial firn thickness in ice-equivalent units.

2.2.3 Numerical aspects

The parameters a, τ and l are discretized onto a fine depth grid called the *age-equation grid*. Equation (1) (for a simple archive) or Equation (2) (for an ice-core archive) are solved using a cumulative sum. Then Equation (4) for the Δ_{depth} is solved to deduce the air age from Equation (3). To solve Equation (4), we first integrate $\frac{D}{\tau}$ from the surface down to every depth in the age-equation grid, i.e. we have a correspondence table between real depths and unthinned-ice-equivalent (UIE) depths. Then, for every

180 actual air depth in the age-equation grid, we obtain the air UIE depth from the table. We then subtract the right-hand side of Equation (4) from this air UIE depth to get the ice UIE depth. Finally, we use the correspondence table to obtain the real ice depth and the Δ_{depth}. When we need to compute the age of the ice or air or Δ_{depth} at depths which are not nodes of the age-equation grid (for example when comparing the model with observations, see below), we use a linear interpolation.

2.3 The probabilistic problem

2.3.1 General probabilistic consideration

The general idea of Paleochrono-1.1 is to combine different sources of chronological information: prior knowledge on the archiving process, together with various chronological observations (e.g. radiometric ages). The assumption is that each site and each site pair (used for stratigraphic links) have independent

190 information. Moreover, within each site and within each site pair, the various types of chronological information are assumed to be independent. For example, for a given site, the prior scenario of the deposition rate, the dated horizons and the dated intervals are all assumed to be independent. It is only within each type of information for a certain site or a certain site pair that it is possible to define the correlation of the information. For prior archiving scenarios of deposition rate (and thinning and LID for

195 an ice core), we do this by defining correlation matrices which have a triangular form, that is, the correlation matrix has ones along its diagonal and the correlation linearly decreases to zero when the age difference (for the deposition rate and LID) or the depth difference (for the thinning function) reaches a user-defined λ value. Setting these correlation matrices for the prior allows to have a weighting which does not depend on the resolution chosen for the inversion grids. As a consequence, the cost function

200 converges towards a single value when the resolution is increased.

In mathematical terms (Tarantola, 2005), combining different sources of information corresponds to multiplying the probability density functions (PDFs) of the prior and of the observations. The result of this multiplication is called the likelihood function. Here, we assume the PDFs to be independent multivariate Gaussian distributions. Multiplying the PDFs therefore corresponds to adding least squares

205 terms.

2.3.2 The least-squares cost function

We write the cost function as follows:

$$J = \sum_k J_k + \sum_{k<m} J_{k,m},$$

(5)

where J_k is the term related to site number k and $J_{k,m}$ is the term related to site pair (k, m).

For a simple archive, the cost function term is the sum of terms related to the age at the top of the sequence

210 χ_0, deposition prior information, dated horizons, and dated intervals. For an ice-core archive, the cost function term is the sum of terms related to the age at the top of the site χ_0, the prior information (for deposition, thinning, and LID), dated horizons (in ice or air), dated intervals (in ice or air), and Δ_{depth} observations.

For a site pair of simple archives, the cost function term simply contains a term related to the stratigraphic

215 links. For a site pair of ice-core archives, the cost function term is the sum of four terms related to ice-ice, ice-air, air-ice and air-air stratigraphic links. For a mixed site pair of a simple archive and an ice-core archive, the cost function term is the sum of two terms related to ice and air stratigraphic links.

Each of additive components of the J_k and $J_{k,m}$ terms described above is written as:

$$J = \boldsymbol{R^T}\, C^{-1}\, \boldsymbol{R}$$

(6)

where $\boldsymbol{R}$ is a residual vector, i.e. a vector containing the differences between the model values and the

220 observations/prior values divided by the uncertainty of the observations/prior, and $\boldsymbol{C}$ is a correlation matrix. This correlation matrix can be Cholesky-decomposed as $\boldsymbol{C = L\, L^T}$, so that Equation (6) can be rewritten:

$$\mathrm{J} = (\boldsymbol{L^{-1}R})^T\, (\boldsymbol{L^{-1}R})$$

(7)

At the end, we therefore have the sum of independent scalar residuals.

2.3.3 The input variables

225 The general idea is to adjust the age of the top of the record and the deposition rate (as well as the thinning function and LID for an ice-core archive) so as to minimize the cost function. We call these variables the *inverted variables*. The prior estimates of deposition rate (and thinning and LID for an ice core) are transferred by interpolation onto the age-equation grid. A first approach could be to adjust these variables

on the same age-equation grid, as is done in the Datice software (Lemieux-Dudon, 2009; Lemieux-Dudon

230   et al., 2010b, a, 2015). This requires the inversion of many variables, hence considerable computing

resources. Here we follow the same approach as in IceChrono (Parrenin et al., 2015), where we define a

multiplicative correction function onto a coarser grid, called the *inversion grid*. These correction functions

are defined as a function of the age for the deposition rate and LID and as a function of the depth for the

thinning function. We then transfer these correction functions on the age-equation grid by a linear

235   interpolation, using the prior age (the age calculated from the prior scenario of deposition, LID and

thinning) for the deposition rate and the LID. A basic assumption of our method is that the inverted

variables are always strictly positive, otherwise the Equations (1-4) have a singularity for a value of zero

for deposition rate and thinning. The correction function should therefore stay strictly positive as well.

Such variables are called *Jeffreys variables* and are generally described by log-normal distributions

240   (Tarantola, 2005). Through the application of a change of variable using the logarithm function, Jeffreys

variables become Cartesian and are then described by Gaussian probabilities.

2.3.4 The optimization method

This least-squares problem is solved iteratively using a *trust region* algorithm (Byrd et al., 1988; Branch

et al., 1999), which converges toward a minimum of the cost function and stops when a convergence

245   criterion is met (the default value is 10^{-5} but it can easily be changed). At each iteration, the model is

linearized, that is, we consider the linear operator which is tangent to the model. This linear system is

solved and the solution is then used as the base of the next iteration.

Contrary to IceChrono, the Jacobian operator is calculated analytically. For each site and each site pair,

the Jacobian matrix is derived for the residuals. For additional efficiency, the linear tangent operator and

250   its adjoint are derived for the multi-site logic. Indeed, when using the linear solver, one does not need to

calculate the Jacobian matrix, but just the effect of this matrix or its transpose on a vector. The linear

tangent and adjoint operators are therefore an efficient way to solve a least-squares problem, especially

when the Jacobian matrix is sparse because this Jacobian matrix does not need to be fully formed.

The initial value of the input vectors is set either as the prior, randomly or from the result of a previous

255   dating experiment. The latter option is possible even if a previous experiment did not have the same depth

or age resolutions. It is therefore possible to use a bootstrap method, starting from a fast, low-resolution experiment to spin and following up with a high-resolution experiment.

The trust region algorithm provides optimized values of the input vectors. At the solution, the product of the transpose Jacobian matrix with itself gives an approximate value of the Hessian matrix, that is, the inverse of the posterior covariance matrix. From there, the covariance matrix of the input variables for each site is calculated. Then, the covariance matrix for the output variables for each site is calculated.

2.4 Programming aspects

Paleochrono-1.1 is coded in the Python 3 programming language with several scientific packages (numpy, scipy, matplotlib). Paleochrono-1.1 both solves the optimization problem and displays the results as figures. For a simple archive, the figures show deposition rate and age. For an ice-core archive, the figures depict deposition rate, thinning function, LID, ice age, air age, Δ_{depth}, Δ_{age}, and ice layer thickness.

We use the trust region algorithm as implemented in the `scipy.optimize.least_squares` function. Compared to IceChrono, several coding optimizations have also been made.

The core of the code is entirely separated from the dating experiment directory which also contains the results of the run and which is composed of general parameter files, a directory for each site (which contains the parameters and observations for the given site) and a directory for each site pair (which contains the observations for the given site pair). Parameters that are common to all sites or site pairs can be set directly in a single file. All the parameter files follow the YAML format (Paleochrono-1.1 uses the pyaml module), which, contrary to IceChrono, allows one to make a clear separation between the main code and the parameters. The input data are given in text files. With respect to IceChrono, all files are given more straightforward names. It is not necessary to understand Python to run the code. Documentation on how to use Paleochrono-1.1 is available within the code. The output figures have also been improved with respect to IceChrono.

There are outputs at each steps of the code, including the initialisations, the optimization, the computing of the confidence intervals and the construction of the graphs, so that the user can inspect the process and estimate how much time is needed for completion. In particular, during the optimization by the trust region algorithm, the value of the cost function and its reduction is displayed at each iteration.

There are no fixed units in the code, so it is possible to use any unit system, but the units must be consistent. For example, it is possible to use kyr as the age unit instead of yr, but then this unit has to be used everywhere. Also, for a particular site, the depth can be expressed in another unit system (e.g., mm for speleothems), but then the deposition rate is expressed using the derived unit (e.g., mm/yr for speleothems).

3. Example dating experiment

IceChrono (Parrenin et al., 2015) was used on the AICC2012 dating experiment, a chronology that combines the EPICA Dome C (EDC), Vostok (VK), Talos Dome (TALDICE) and EPICA Dronning Maud Land (EDML) Antarctic ice cores and the NorthGRIP (NGRIP) Greenland ice core (Bazin et al., 2013; Veres et al., 2013).

Paleochrono-1.1 was already used on the AICC2023 dating experiment (Bouchet et al., 2023), an incremental improvement of AICC2012, with updated prior scenarios and dated horizons for the EDC ice core over the last 800 kyr. For this experiment, we increased the resolution until the cost function converges towards a single value. This value is ~196, which is small with respect to the number of observations (2,139), highlighting the good general match of the posterior scenario with respect to the observations.

Here, to test and demonstrate the ability of Paleochrono-1.1 to date simple archives in combination with ice cores, we incorporate into this AICC2023 experiment two last glacial speleothems (MSD and MSL) from Hulu Cave (Wang et al., 2001), that have U/Th dated horizons (Cheng et al., 2018) on a 18-55 ka BP time interval. We caution readers that this dating experiment has been constructed to test the Paleochrono-1.1 model and to illustrate its abilities, and as such the resulting chronology presented here is *not* intended to be used for paleoclimatic studies. A future effort to update the AICC2023 chronology with information from speleothems is planned, but this is beyond the scope of the current study.

We set the prior deposition scenario to constant for both speleothems with an relative uncertainty (1σ) set to 1 (that is, the deposition is allowed to vary by an exponential factor). This value of 1 was defined by an *a posteriori* analysis of the reconstructed deposition rate and its variations. We assume also a

correlation length of 1,000 yr for the deposition rate of both speleothems, assuming higher frequency

310   variations are absent. For each speleothem, we use published U/Th dated horizons (Cheng et al., 2018).

Then, we define stratigraphic links between (1) the NGRIP $\delta^{18}O_{ice}$ and the MSD $\delta^{18}O_{calcite}$, (2) the MSD

and MSL $\delta^{18}O_{calcite}$ and (3) the MSL $\delta^{18}O_{calcite}$ and the EDC CH_4 records. To do so, we take advantage of

the fact that the abrupt climate variability characterising the last glacial period (NorthGRIP project

members, 2004; Corrick et al., 2020) is clearly expressed in each of these records. We link the records at

315   the onset of each abrupt Dansgaard-Oeschger (DO) events (Figure 2) using a mid-slope approach by

assuming a global synchroneity in the timing of the rapid warming transitions and of the $\delta^{18}O_{calcite}$ changes

(Corrick et al., 2020). We assign a constant uncertainty (1σ) of 100 yr to these synchronisation horizons.

100 yr is a rough estimate of the synchronisation error during DO transitions. A more careful analysis

would be needed to refine these estimates individually, but this is beyond the scope of the current

320   manuscript.

We call this experiment *AICC2023-Hulu*. Figure 2 shows the NGRIP $\delta^{18}O_{ice}$ record, Hulu/MSD and

Hulu/MSL $\delta^{18}O_{calcite}$ records and EDC CH_4 record onto this common and optimized age scale. Figure 3

are automatically generated by the Paleochrono-1.1 software and represent the chronology and deposition

rate for the MSL speleothem as well as the synchronisation for the NGRIP-MSD site pair, respectively.

325   We can observe in Figure 3 that the posterior chronology for the MSL speleothem is in better agreement

with the dated horizons than the prior chronology (which is expected since a constant growth rate is

assumed in the prior case) and generally fits the U-Th ages within their confidence interval. Paleochrono-

1.1 is also able to interpolate in-between age horizons when they are less dense. The uncertainty of the

posterior chronology ranges from 50 to 400 yr (1σ), increasing when the age horizons are less dense or

330   less precise.

Figure 4 shows that Paleochrono-1.1 is able to reconstruct a variable deposition rate from the

chronological information, in particular the dated horizons along the MSL speleothem. It is also able to

estimate an uncertainty on this posterior reconstruction, which will depend mainly on the uncertainty of

the U/Th dated horizons, the depth resolution of the U/Th dates and the assumed growth-rate variation

335   that affects interpolation uncertainty.

In Figure 5, we observe that Paleochrono-1.1 starts with a prior scenario based on archiving models with asynchronous stratigraphic links and that this new tool is able to come up with a solution where these stratigraphic links are respected.

4. Benchmarks

340 We now test the computing performance of Paleochrono-1.1 (computing time, memory used) in various dating experiments and configurations. We use a computing server with a Bi pro Xeon 2.10 GHz (48 cores and 96 threads) and 256 Gb of RAM. We use the Anaconda distribution of Python, which contains the Intel MKL (Math Kernel Library), providing parallel algorithms for common mathematical operations.

4.1 Comparison to IceChrono

345

We perform a test of computing performances on the AICC2012-VHR (Very High Resolution) experiment as defined in Parrenin et al. (2015). In this experiment, there are 10,520 variables to be inverted and 1,939 observations.

The experiment took about 24h and used 4.8 GB of RAM using IceChrono. The same experiment took 2 350 m and used 3.6 GB of RAM using Paleochrono-1.1. This is a factor ~700 difference in computing time and 25% less memory. This improvement in terms of computing resources will allow users to increase the number of sites in a dating experiment, increase the resolution within a paleoclimatic site, and/or run the software on their desktop computer rather than on a server.

4.2 Computing time as a function of the number of computing cores

355 We now test the Paleochrono-1.1 software with different numbers of computing cores. We use the AICC2023 dating experiment as defined in section 3. We test with 1, 2, 4, 6, 8, 12, 16, 24, 32 and 48 computing cores. Figure 6 shows the result of this experiment. The total computing time (resp. optimization time) ranges from 3 m 50 s (resp. 1 m 51 s) for 48 computing cores, to 24 mn (resp. 2 m 55 s) for one computing core. In this dating experiment, the Paleochrono-1.1 software therefore scales quite 360 well from one core to 16 cores (with a scaling factor of ~6), but after 16 cores the computing time

stagnates. In this experiment, 16 therefore seems to be the optimal number of computing cores, but this result might depend on the number of inverted parameters in the dating experiment.

4.3 Resources as a function of the number of inverted parameters

365 We now test the resources required by Paleochrono-1.1 as a function of the number of inverted parameters. We use the AICC2023 dating experiment (Bouchet et al., 2023). Starting from a low-resolution experiment, we multiply the resolution of deposition rate, LID and thinning in this experiment by factors of: 1, 2, 5 and 10. As a result, the number of inverted parameters is: 6,478, 12,944, 32,332 and 64,644. The third experiment corresponds to the official AICC2023 experiment (Bouchet et al., 2023). The results are shown on Figure 7 (on a log scales). The computing time ranges from ~0.7 m to ~14.2 m.

370 The memory used ranges from ~2.1 GB to ~107.3 GB. We can observe that the memory evolves roughly quadratically as a function of the number of inverted parameters. For the computing time, the evolution is close to linear for a small number of parameters and then becomes quadratic for a large number of parameters.

5 Discussion and perspectives

375 ## 5.1 On the use of probabilistic dating methods

First, we discuss why we should combine chronologies in the first place and what "optimal" means in this context. Common chronologies with internally-consistent sources of chronological information have the advantage to be more accurate because they incorporate more data and their uncertainties. A probabilistic method can capitalize on the fact that each dating method has its own strengths and they are

380 complementing each other. In the example employed here, the speleothems provide very accurate absolute ages via radiometric U/Th dating, whereas the NGRIP ice core provides very accurate relative ages (i.e., durations) from counting of annual layers across intervals. Combining these two archives could therefore provide a chronology that is more accurate than the age scale of each archive dated in isolation. Moreover, common chronologies allow to decipher temporal sequence of climate and environmental changes

385   between different archives as lead and lags are not originating from chronology differences (assuming the synchronization links are realistic).

Second, we enumerate several applications of probabilistic dating models. Datice, the predecessor of Paleochrono-1.1, was used to create a coherent chronology of the EDC, EDML and NGRIP ice cores during the last deglaciation (Lemieux-Dudon et al., 2010b). Later, Datice was used to build AICC2012

390   (Bazin et al., 2013; Veres et al., 2013), a common chronology for 4 Antarctic ice cores (EDC, VK, EDML, TALDICE) and one Greenland ice core (NGRIP), taking into account many different types of absolute or relative chronological constraints. AICC2012 was used to discuss the comparison and phasing of EDC, EDML, TALDICE and NGRIP during the DO events of the last deglaciation (Landais et al., 2015). Datice was also used in a multi-archives context to build a coherent chronological scenario in the Mediterranean

395   region during the last deglaciation for 3 lake-sediments cores, 2 speleothems and one marine core (Bazin et al., 2019). More recently, Paleochrono-1.1 was used to build the DF2021 chronology for the Dome Fuji ice core (Oyabu et al., 2022), taking into account dated horizons and Δdepth constraints from various methods. Paleochrono-1.1 was also used to reconstruct the temporal variations of surface mass balance around Dome Fuji (Antarctica) for the last 5,000 years using shallow ice cores and snow pits (Oyabu et

400   al., 2023) synchronized using volcanic horizons. The ST22 chronology of the Skytrain ice core was constructed by matching its stratigraphy to EDC through various ice and air records and by using Paleochrono-1.1 to obtain a best fit. Finally, AICC2023, an update of AICC2012 with in-particular more accurate orbital-tuning records, was recently build using Paleochrono-1.1 (Bouchet et al., 2023).

Third, we discuss the limitation of probabilistic dating methods. Common chronologies are also attached

405   to drawbacks: they may mask systematic differences between dating methods that should be investigated and solved rather than forced into the same framework. In this case, the optimal solution in probabilistic terms may actually represent a compromise that is less physically meaningful. Additionally, the models for combining all the information may grow to be so comprehensive that most users will not be able to maintain an overview of the data employed, and operating the model will entail sometimes implicit and

410   important choices, e.g. on how to estimate the error bars of the prior and of the observations, how to set the correlation lengths for the prior, etc.

Another limitation of the method is that it requires errors to be both independent and have Gaussian distribution. Radiocarbon calendar ages typically do not have a Gaussian uncertainty, as they are a convolution of the measurement uncertainty and a calibration curve taking into account the variable atmospheric ¹⁴C history. Likewise, volcanic ties have a complex uncertainty: if the tie correctly links the same layer in two records, the uncertainty of the synchronization will usually be no more than a few years, determined by data resolution and the shape of the signal matched. However, if the tie is incorrect, the error can be any number, and the error will rarely be described well by a Gaussian distribution with a width of e.g. 200 years. Furthermore, errors in any type of age constraint will be correlated in case of systematic biases. For example, when a sequence of closely spaced volcanic layers (forming a recognizable pattern due to their similar spacing) are matched between two ice cores, the tie points are likely all correct or all erroneous, making their uncertainties highly correlated. In the experiment performed here, there may be temporal lags in the climate system between the various parameters that are stratigraphically linked, the annual layer counting could systematically over- or under-count layers beyond what is included in the counting uncertainties, and the U/Th dating may have systematic biases related to for example the detrital Th correction.

In conclusion, optimal chronologies are practical for users who want to use the best possible common chronology, but it absolutely does not replace the need to compare and improve the chronologies of individual sites. The compromises involved in the modelling entail a risk that wrong chronological information or insufficiently quantified uncertainties will influence the resulting time scale negatively in a non-transparent way.

5.2 Comparison with IceChrono

Paleochrono-1.1 is an evolution of IceChrono (Parrenin et al., 2015), since it started as the same code base. But Paleochrono-1.1 improves several aspects of IceChrono. The first improvement to note is that Paleochrono-1.1 can handle continuous paleoclimatic archives other than ice cores. We showed here a test with two speleothems from Hulu Cave and multiple ice cores from Greenland and Antarctica. Other improvements include:

- **Efficiency:** Paleochrono-1.1 uses significantly less computing resources, in particular computing time. This is thanks to:

  o the new trust region algorithm which can use an iterative solver at each linear iteration

  o the per-site analytical Jacobian matrix

  o the prior and multi-sites linear tangent and adjoint operators

  o the ability to define the convergence criterion

  o various python optimizations

  On a AICC2012-VHR dating experiment identical to the one shown in Parrenin et al. (2015), the gain in computation time is a factor ~700, which is huge. Therefore, Paleochrono-1.1 is more adapted for high-resolution runs than IceChrono. The memory reduction is less significant, with only a 25% reduction.

- **Ease of use:** Paleochrono-1.1 is easier to use than IceChrono thanks to several improvements:

  o Paleochrono-1.1 now uses parameters files in the YAML format instead of the python format. This makes it easier to work with these parameter files and creates a clear separation between the main code and the parameters.

  o Paleochrono-1.1 now uses a simpler naming of parameters and input/output files.

  o Paleochrono-1.1 now has pre-defined grid types. Apart from the 'regular' type with a constant step, there is a 'quadratic' type with a linearly increasing step. It is also easy to add new grid types. This makes it easier to have, for example, age grids which are refined for present times and coarse for past times, or depths grids for ice cores which are more refined near the bedrock.

  o There is an interactive output during the optimization process that displays the evolution of the cost function at each iteration. This makes it easier to inspect the optimization process and estimate the time that is still needed for the run to complete.

  o The output figures have been greatly improved. In particular, the resolution is displayed on the deposition rate, LID and thinning figures. Moreover, it is possible to define the units used and the figures will respect these units.

465 • **Accuracy:** Paleochrono-1.1 is more accurate than IceChrono because of the following improvements:

○ Paleochrono-1.1 now inverts χ_0, the age at the top of the sequence, while it was prescribed in IceChrono. This is an improvement since it is not always possible to accurately determine the age of the top of the sequence, in which case it needs to be estimated within

470 the optimization process.

○ The forward model is more accurate, thanks to several inaccuracies which have been corrected.

○ Paleochrono-1.1 does not estimate the thinning in the firn for Equation (4) but directly prescribes $\left.\frac{D}{T}\right|_{firn}^{0}$. This allows Equation (4) to be exact instead of being an approximation.

475 ○ Thanks to the analytical Jacobian, the optimization finds a better minimum, that is, in closer agreement with the observations.

In summary, Paleochrono-1.1 is a considerable improvement with respect to IceChrono and we highly recommend the use of Paleochrono-1.1 to any existing and interested users of IceChrono. Indeed, the future maintenance of IceChrono will be discontinued.

480 ## 5.3 Computing resources

In the AICC2023 dating experiment, we have tested the computed time needed by Paleochrono-1.1 as a function of the number of computing cores used. We find that 16 seems to be the optimal number of computing cores, with a code which scales with a factor ~6 with respect to one unique computing core. We have successfully tested the Paleochrono-1.1 software in the AICC2023 experiment with ~65,000

485 inverted parameters and ~2,000 observations. We find that the resource requirement (computing time, memory) evolves roughly quadratically as a function of the number of inverted parameters. In this experiment, the limiting factor is the memory. Indeed, the most demanding run takes only 14 mn, which is acceptable but the memory used (107 GB) is on the upper range of what can be found in a workstation. Using a computing node with ~ 1TB of memory, which is at the edge of what can be done currently with

490 shared memory, would allow one to invert for ~200,000 parameters.

5.4 Possible future improvements

Paleochrono-1.1 only deals with continuous depth-age models. It could be interesting in the future to include possible hiatuses.

Paleochrono-1.1 does not support the automatically detection of outliers in the original site and site pair
495 chronological information, e.g. information that is incompatible (within uncertainty) with the remaining constraints. A posterior visual check is necessary to detect them, and the irrelevant chronological observations should be manually removed.

Regarding resources, the most memory-demanding part in this run is not the optimization itself, but rather the construction of the posterior covariance matrix, which is required to evaluate the uncertainty of the
500 posterior scenario. Another possibility to decrease the memory used and further increase the number of inverted parameters would be to not form the whole posterior covariance matrix, but only subsets of it, as seems possible using the LSQR linear solver (Kostina et al., 2009).

Conclusions

Here we describe a new probabilistic dating model for continuous climate archives, called *Paleochrono-*
505 *1.1*. Paleochrono-1.1 is an evolution of the IceChrono model originally dedicated to ice cores, but it can now handle other continuous climate archives based on a varying deposition rate, such as lake and marine sediment cores or speleothems, and produce a coherent age scale between these multiple records and archives. Paleochrono-1.1 is more efficient, easier to use and more accurate than IceChrono. We demonstrate the ability of Paleochrono-1.1 in an AICC2023-Hulu dating experiment where we add two
510 radiometrically-dated speleothems from Hulu Cave to the AICC2023 dating experiment (Bouchet et al., 2023). We then benchmark the computing resources needed to run Paleochrono-1.1. We observe that the code scales with up 16 cores with a gain factor ~6. We also show that the computing time and memory evolve roughly quadratically with respect to the number of inverted parameters. Finally, we test an AICC2023 dating experiment with ~65,000 parameters, where the limiting factor is the memory used.
515 Going beyond 200,000 inverted parameters would require rewriting some sections of the model, in

particular with respect to the computation of the posterior covariance matrix needed to compute the uncertainty of the posterior scenario.

Paleochrono-1.1 has already been used in several published studies, either on one unique ice-core site but with multiple age constrains (Oyabu et al., 2022) or with multiple ice-core sites and multiple age constrains (Oyabu et al., 2023; Mulvaney et al., 2023; Bouchet et al., 2023). Many other applications of Paleochrono-1.1 would be possible for various time periods and using various paleoclimatic records.

Code availability

Paleochrono-1.1 is an open source model available under the MIT license. It is hosted on the github facility (https://github.com/parrenin/paleochrono) and the version corresponding to the submission of this manuscript has been published on Zenodo (https://doi.org/10.5281/zenodo.10580279). The main author (F. Parrenin) can provide support for people wanting to use the software.

Author contribution

FP developed the model code. MB, AL, KK, IO and RM tested the software. FP ran the simulations which were discussed between all co-authors. FP prepared the manuscript with contributions from all co-authors.

Competing interests

The authors declare they have no conflict of interest.

Acknowledgements.

We thank Lucie Bazin for helpful discussions and for testing the Paleochrono-1.1 software. This work was supported by the Fondation Ars et Cuttoli CO2Role project and by the LEFE IceChrono and CO2Role projects. Some preliminary computations presented in this paper were performed using the GRICAD infrastructure (https://gricad.univ-grenoble-alpes.fr), which is supported by Grenoble research communities. EC acknowledges the financial support from the French National Research Agency under

the "Programme d'Investissements d'Avenir" through the Make Our Planet Great Again HOTCLIM project (ANR-19-MPGA-0001). SOR gratefully acknowledges the support from the Carlsberg Foundation to the ChronoClimate project . CB acknowledges financial support from the US National Science Foundation (grants 1643394 and 1702920). We are thankful to Anders Svensson for helpful discussions.

References

Bazin, L., Landais, A., Lemieux-Dudon, B., Toyé Mahamadou Kele, H., Veres, D., Parrenin, F., Martinerie, P., Ritz, C., Capron, E., Lipenkov, V., Loutre, M.-F., Raynaud, D., Vinther, B., Svensson, A., Rasmussen, S. O., Severi, M., Blunier, T., Leuenberger, M., Fischer, H., Masson-Delmotte, V., Chappellaz, J., and Wolff, E.: An optimized multi-proxy, multi-site Antarctic ice and gas orbital chronology (AICC2012): 120–800 ka, Clim Past, 9, 1715–1731, https://doi.org/10.5194/cp-9-1715-2013, 2013.

Bazin, L., Lemieux-Dudon, B., Siani, G., Govin, A., Landais, A., Genty, D., Michel, E., and Nomade, S.: Construction of a tephra-based multi-archive coherent chronological framework for the last deglaciation in the Mediterranean region, Quat. Sci. Rev., 216, 47–57, https://doi.org/10.1016/j.quascirev.2019.05.018, 2019.

Bouchet, M., Landais, A., Grisart, A., Parrenin, F., Prié, F., Jacob, R., Fourré, E., Capron, E., Raynaud, D., Lipenkov, V. Y., Loutre, M.-F., Extier, T., Svensson, A., Legrain, E., Martinerie, P., Leuenberger, M., Jiang, W., Ritterbusch, F., Lu, Z.-T., and Yang, G.-M.: The Antarctic Ice Core Chronology 2023 (AICC2023) chronological framework and associated timescale for the European Project for Ice Coring in Antarctica (EPICA) Dome C ice core, Clim. Past, 19, 2257–2286, https://doi.org/10.5194/cp-19-2257-2023, 2023.

Branch, M. A., Coleman, T. F., and Li, Y.: A Subspace, Interior, and Conjugate Gradient Method for Large-Scale Bound-Constrained Minimization Problems, SIAM J. Sci. Comput., 21, 1–23, https://doi.org/10.1137/S1064827595289108, 1999.

Brauer, A., Hajdas, I., Blockley, S. P. E., Bronk Ramsey, C., Christl, M., Ivy-Ochs, S., Moseley, G. E., Nowaczyk, N. N., Rasmussen, S. O., Roberts, H. M., Spötl, C., Staff, R. A., and Svensson, A.: The importance of independent chronology in integrating records of past climate change for the 60–8 ka INTIMATE time interval, Quat. Sci. Rev., 106, 47–66, https://doi.org/10.1016/j.quascirev.2014.07.006, 2014.

Byrd, R. H., Schnabel, R. B., and Shultz, G. A.: Approximate solution of the trust region problem by minimization over two-dimensional subspaces, Math. Program., 40, 247–263, https://doi.org/10.1007/BF01580735, 1988.

Cheng, H., Edwards, R. L., Southon, J., Matsumoto, K., Feinberg, J. M., Sinha, A., Zhou, W., Li, H., Li, X., Xu, Y., Chen, S., Tan, M., Wang, Q., Wang, Y., and Ning, Y.: Atmospheric $^{14}C/^{12}C$ changes during the last glacial period from Hulu Cave, Science, 362, 1293–1297, https://doi.org/10.1126/science.aau0747, 2018.

Corrick, E. C., Drysdale, R. N., Hellstrom, J. C., Capron, E., Rasmussen, S. O., Zhang, X., Fleitmann, D., Couchoud, I., and Wolff, E.: Synchronous timing of abrupt climate changes during the last glacial period, Science, 369, 963–969, https://doi.org/10.1126/science.aay5538, 2020.

Dome Fuji Ice Core Project Members, Kawamura, K., Abe-Ouchi, A., Motoyama, H., Ageta, Y., Aoki, S., Azuma, N., Fujii, Y., Fujita, K., Fujita, S., Fukui, K., Furukawa, T., Furusaki, A., Goto-Azuma, K., Greve, R., Hirabayashi, M., Hondoh, T., Hori, A., Horikawa, S., Horiuchi, K., Igarashi, M., Iizuka, Y., Kameda, T., Kanda, H., Kohno, M., Kuramoto, T., Matsushi, Y., Miyahara, M., Miyake, T., Miyamoto, A., Nagashima, Y., Nakayama, Y., Nakazawa, T., Nakazawa, F., Nishio, F., Obinata, I., Ohgaito, R., Oka, A., Okuno, J., Okuyama, J., Oyabu, I., Parrenin, F., Pattyn, F., Saito, F., Saito, T., Saito, T., Sakurai, T., Sasa, K., Seddik, H., Shibata, Y., Shinbori, K., Suzuki, K., Suzuki, T., Takahashi, A., Takahashi, K., Takahashi, S., Takata, M., Tanaka, Y., Uemura, R., Watanabe, G., Watanabe, O., Yamasaki, T., Yokoyama, K., Yoshimori, M., and Yoshimoto, T.: State dependence of climatic instability over the past 720,000 years from Antarctic ice cores and climate modeling, Sci. Adv., 3, e1600446, https://doi.org/10.1126/sciadv.1600446, 2017.

Elderfield, H., Ferretti, P., Greaves, M., Crowhurst, S., McCave, I. N., Hodell, D., and Piotrowski, A. M.: Evolution of Ocean Temperature and Ice Volume Through the Mid-Pleistocene Climate Transition, Science, 337, 704–709, https://doi.org/10.1126/science.1221294, 2012.

EPICA community members, Augustin, L., Barbante, C., Barnes, P. R. F., Marc Barnola, J., Bigler, M., Castellano, E., Cattani, O., Chappellaz, J., Dahl-Jensen, D., Delmonte, B., Dreyfus, G., Durand, G., Falourd, S., Fischer, H., Flückiger, J., Hansson, M. E., Huybrechts, P., Jugie, G., Johnsen, S. J., Jouzel, J., Kaufmann, P., Kipfstuhl, J., Lambert, F., Lipenkov, V. Y., Littot, G. C., Longinelli, A., Lorrain, R., Maggi, V., Masson-Delmotte, V., Miller, H., Mulvaney, R., Oerlemans, J., Oerter, H., Orombelli, G., Parrenin, F., Peel, D. A., Petit, J.-R., Raynaud, D., Ritz, C., Ruth, U., Schwander, J., Siegenthaler, U., Souchez, R., Stauffer, B., Peder Steffensen, J., Stenni, B., Stocker, T. F., Tabacco, I. E., Udisti, R., van de Wal, R. S. W., van den Broeke, M., Weiss, J., Wilhelms, F., Winther, J.-G., Wolff, E. W., and Zucchelli, M.: Eight glacial cycles from an Antarctic ice core, Nature, 429, 623–628, https://doi.org/10.1038/nature02599, 2004.

EPICA Community Members, Barbante, C., Barnola, J.-M., Becagli, S., Beer, J., Bigler, M., Boutron, C., Blunier, T., Castellano, E., Cattani, O., Chappellaz, J., Dahl-Jensen, D., Debret, M., Delmonte, B., Dick, D., Falourd, S., Faria, S., Federer, U., Fischer, H., Freitag, J., Frenzel, A., Fritzsche, D., Fundel, F.,

605 Gabrielli, P., Gaspari, V., Gersonde, R., Graf, W., Grigoriev, D., Hamann, I., Hansson, M., Hoffmann, G., Hutterli, M. A., Huybrechts, P., Isaksson, E., Johnsen, S., Jouzel, J., Kaczmarska, M., Karlin, T., Kaufmann, P., Kipfstuhl, S., Kohno, M., Lambert, F., Lambrecht, A., Lambrecht, A., Landais, A., Lawer, G., Leuenberger, M., Littot, G., Loulergue, L., Lüthi, D., Maggi, V., Marino, F., Masson-Delmotte, V., Meyer, H., Miller, H., Mulvaney, R., Narcisi, B., Oerlemans, J., Oerter, H., Parrenin, F., Petit, J.-R.,
610 Raisbeck, G., Raynaud, D., Röthlisberger, R., Ruth, U., Rybak, O., Severi, M., Schmitt, J., Schwander, J., Siegenthaler, U., Siggaard-Andersen, M.-L., Spahni, R., Steffensen, J. P., Stenni, B., Stocker, T. F., Tison, J.-L., Traversi, R., Udisti, R., Valero-Delgado, F., van den Broeke, M. R., van de Wal, R. S. W., Wagenbach, D., Wegner, A., Weiler, K., Wilhelms, F., Winther, J.-G., and Wolff, E.: One-to-one coupling of glacial climate variability in Greenland and Antarctica, Nature, 444, 195–198,
615 https://doi.org/10.1038/nature05301, 2006.

Hodell, D. A., Brenner, M., Kanfoush, S. L., Curtis, J. H., Stoner, J. S., Xueliang, S., Yuan, W., and Whitmore, T. J.: Paleoclimate of Southwestern China for the Past 50,000 yr Inferred from Lake Sediment Records, Quat. Res., 52, 369–380, https://doi.org/10.1006/qres.1999.2072, 1999.

Kostina, E. A., Saunders, M. A., and Schierle, I.: Computation of covariance matrices for constrained
620 parameter estimation problems using LSQR, Univ., 2009.

Landais, A., Masson-Delmotte, V., Stenni, B., Selmo, E., Roche, D. M., Jouzel, J., Lambert, F., Guillevic, M., Bazin, L., Arzel, O., Vinther, B., Gkinis, V., and Popp, T.: A review of the bipolar see–saw from synchronized and high resolution ice core water stable isotope records from Greenland and East Antarctica, Quat. Sci. Rev., 114, 18–32, https://doi.org/10.1016/j.quascirev.2015.01.031, 2015.

625 Laskar, J., Robutel, P., Joutel, F., Gastineau, M., Correia, A. C. M., and Levrard, B.: A long-term numerical solution for the insolation quantities of the Earth, Astron. Astrophys., 428, 261–285, https://doi.org/10.1051/0004-6361:20041335, 2004.

Lemieux-Dudon, B.: Conjonction de données et de modèles pour la datation des forages profonds d'Antarctique et du Groenland, PhD thesis, Université Joseph Fourier, 2009.

630 Lemieux-Dudon, B., Parrenin, F., and Blayo, E.: A Probabilistic Method to Construct an Optimal Ice Chronology for Ice Cores, in: Physics of Ice Core Records 2, 233–245, 2010a.

Lemieux-Dudon, B., Blayo, Petit, J. R. E., Waelbroeck, C., Svensson, A., Ritz, C., Barnola, J.-M., Narcisi, B. M., and Parrenin, F.: Consistent dating for Antarctica and Greenland ice cores, Quat Sci Rev, 29, 8–20, 2010b.

635 Lemieux-Dudon, B., Bazin, L., Landais, A., Toyé Mahamadou Kele, H., Guillevic, M., Kindler, P., Parrenin, F., and Martinerie, P.: Implementation of counted layers for coherent ice core chronology, Clim. Past, 11, 959–978, https://doi.org/10.5194/cp-11-959-2015, 2015.

Lisiecki, L. E. and Raymo, M. E.: A Plio-Pleistocene Stack of 57 Globally Distributed Benthic δ^{18}O Records, Paleoceanography, 20, PA1003, https://doi.org/10.1029/2004PA001071, 2005.

640 Mulvaney, R., Wolff, E. W., Grieman, M. M., Hoffmann, H. H., Humby, J. D., Nehrbass-Ahles, C., Rhodes, R. H., Rowell, I. F., Parrenin, F., Schmidely, L., Fischer, H., Stocker, T. F., Christl, M., Muscheler, R., Landais, A., and Prié, F.: The ST22 chronology for the Skytrain Ice Rise ice core – Part 2: An age model to the last interglacial and disturbed deep stratigraphy, Clim. Past, 19, 851–864, https://doi.org/10.5194/cp-19-851-2023, 2023.

645 NEEM community Members: Eemian interglacial reconstructed from a Greenland folded ice core, Nature, 493, 489–494, https://doi.org/10.1038/nature11789, 2013.

NorthGRIP project members: High-resolution record of Northern Hemisphere climate extending into the last interglacial period, Nature, 431, 147–151, 2004.

Oyabu, I., Kawamura, K., Buizert, C., Parrenin, F., Orsi, A., Kitamura, K., Aoki, S., and Nakazawa, T.: 650 The Dome Fuji ice core DF2021 chronology (0–207 kyr BP), Quat. Sci. Rev., 294, 107754, https://doi.org/10.1016/j.quascirev.2022.107754, 2022.

Oyabu, I., Kawamura, K., Fujita, S., Inoue, R., Motoyama, H., Fukui, K., Hirabayashi, M., Hoshina, Y., Kurita, N., Nakazawa, F., Ohno, H., Sugiura, K., Suzuki, T., Tsutaki, S., Abe-Ouchi, A., Niwano, M., Parrenin, F., Saito, F., and Yoshimori, M.: Temporal variations of surface mass balance over the last 5000 655 years around Dome Fuji, Dronning Maud Land, East Antarctica, Clim. Past, 19, 293–321, https://doi.org/10.5194/cp-19-293-2023, 2023.

Parrenin, F., Rémy, F., Ritz, C., Siegert, M., and Jouzel, J.: New modelling of the Vostok ice flow line and implication for the glaciological chronology of the Vostok ice core, J Geophys Res, 109, D20102, https://doi.org/10.1029/2004JD004561, 2004.

660 Parrenin, F., Dreyfus, G., Durand, G., Fujita, S., Gagliardini, O., Gillet, F., Jouzel, J., Kawamura, K., Lhomme, N., Masson-Delmotte, V., Ritz, C., Schwander, J., Shoji, H., Uemura, R., Watanabe, O., and Yoshida, N.: 1-D-ice flow modelling at EPICA Dome C and Dome Fuji, East Antarctica, Clim Past, 3, 243–259, https://doi.org/10.5194/cp-3-243-2007, 2007.

Parrenin, F., Barker, S., Blunier, T., Chappellaz, J., Jouzel, J., Landais, A., Masson-Delmotte, V., 665 Schwander, J., and Veres, D.: On the gas-ice depth difference (Δdepth) along the EPICA Dome C ice core, Clim Past, 8, 1239–1255, https://doi.org/10.5194/cp-8-1239-2012, 2012.

Parrenin, F., Bazin, L., Capron, E., Landais, A., Lemieux-Dudon, B., and Masson-Delmotte, V.: IceChrono1: a probabilistic model to compute a common and optimal chronology for several ice cores, Geosci Model Dev, 8, 1473–1492, https://doi.org/10.5194/gmd-8-1473-2015, 2015.

670 Shackleton, N. J.: The 100,000-Year Ice-Age Cycle Identified and Found to Lag Temperature, Carbon Dioxide, and Orbital Eccentricity, Science, 289, 1897–1902, 2000.

Shackleton, N. J., Hall, M. A., and Vincent, E.: Phase relationships between millennial-scale events 64,000-24,000 years ago, Paleoceanography, 15, 565–569, 2000.

Sigl, M., Fudge, T. J., Winstrup, M., Cole-Dai, J., Ferris, D., McConnell, J. R., Taylor, K. C., Welten, K.
675 C., Woodruff, T. E., Adolphi, F., Bisiaux, M., Brook, E. J., Buizert, C., Caffee, M. W., Dunbar, N. W., Edwards, R., Geng, L., Iverson, N., Koffman, B., Layman, L., Maselli, O. J., McGwire, K., Muscheler, R., Nishiizumi, K., Pasteris, D. R., Rhodes, R. H., and Sowers, T. A.: The WAIS Divide deep ice core WD2014 chronology – Part 2: Annual-layer counting (0–31 ka BP), Clim Past, 12, 769–786, https://doi.org/10.5194/cp-12-769-2016, 2016.

680 Svensson, A., Andersen, K. K., Bigler, M., Clausen, H. B., Dahl-Jensen, D., Davies, S. M., Johnsen, S. J., Muscheler, R., Parrenin, F., Rasmussen, S. O., Röthlisberger, R., Seierstad, I., Steffensen, J. P., and Vinther, B. M.: A 60 000 year Greenland stratigraphic ice core chronology, Clim Past, 4, 47–57, 2008.

Tarantola, A.: Inverse problem theory and methods for model parameter estimation, Society for Industrial Mathematics, 2005.

685 Veres, D., Bazin, L., Landais, A., Toyé Mahamadou Kele, H., Lemieux-Dudon, B., Parrenin, F., Martinerie, P., Blayo, E., Blunier, T., Capron, E., Chappellaz, J., Rasmussen, S. O., Severi, M., Svensson, A., Vinther, B., and Wolff, E. W.: The Antarctic ice core chronology (AICC2012): an optimized multi-parameter and multi-site dating approach for the last 120 thousand years, Clim Past, 9, 1733–1748, https://doi.org/10.5194/cp-9-1733-2013, 2013.

690 WAIS Divide Project Members: Onset of deglacial warming in West Antarctica driven by local orbital forcing, Nature, 500, 440–444, https://doi.org/10.1038/nature12376, 2013.

Wang, Y. J., Cheng, H., Edwards, R. L., An, Z. S., Wu, J. Y., Shen, C. C., and Dorale, J. A.: A high-resolution absolute-dated late Pleistocene Monsoon record from Hulu Cave, China., Science, 294, 2345–2348, 2001.

695 Williams, D. F., Peck, J., Karabanov, E. B., Prokopenko, A. A., Kravchinsky, V., King, J., and Kuzmin, M. I.: Lake Baikal record of continental climate response to orbital insolation during the past 5 million years, Science, 278, 1114–1117, 1997.
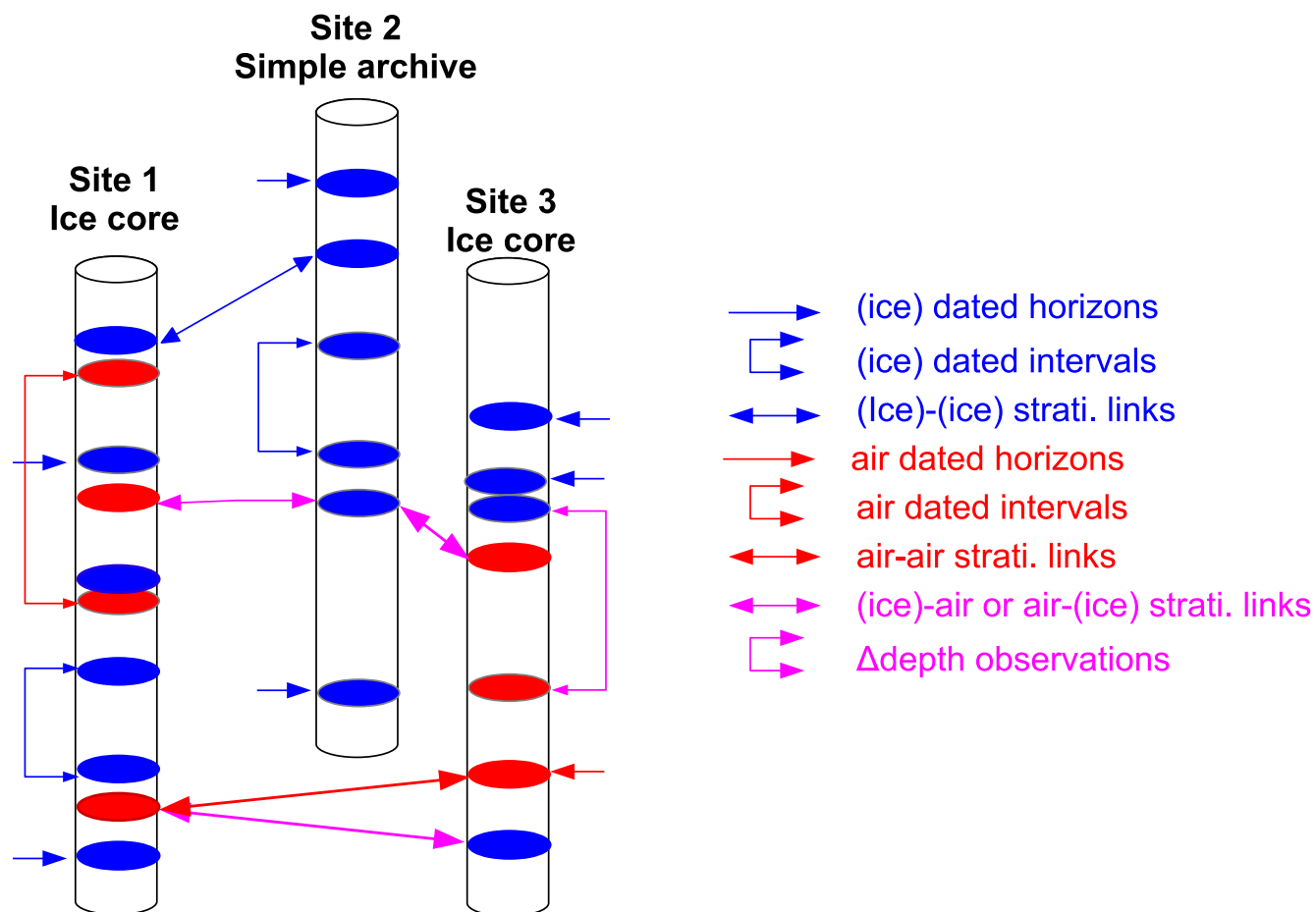
700   Figure 1: Scheme illustrating the different kinds of observations used to constrain the chronologies of the paleoclimatic sites in the Paleochrono-1.1 probabilistic dating model.
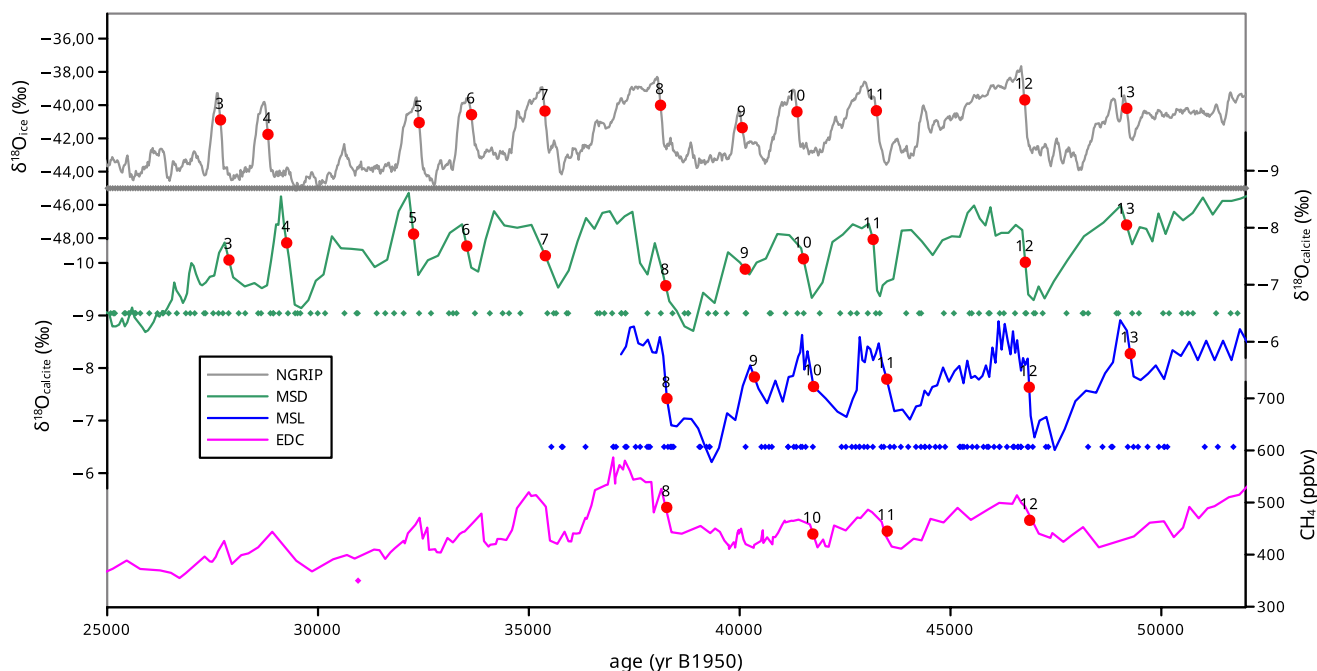
Figure 2: Illustration of the synchronized and optimized chronology AICC2023-Hulu. From Top to bottom: NGRIP $\delta^{18}O_{ice}$ record; Hulu/MSD and Hulu/MSL $\delta^{18}O_{calcite}$ records; EDC CH_4 record. The red dots indicate the mid-points of DO onsets where the stratigraphic links are placed for the NGRIP-MSD, MSD-MSL and MSL-EDC site pairs and the labels indicate the DO numbers. The diamonds at the bottom of each panel represent the dated horizons used for each site.
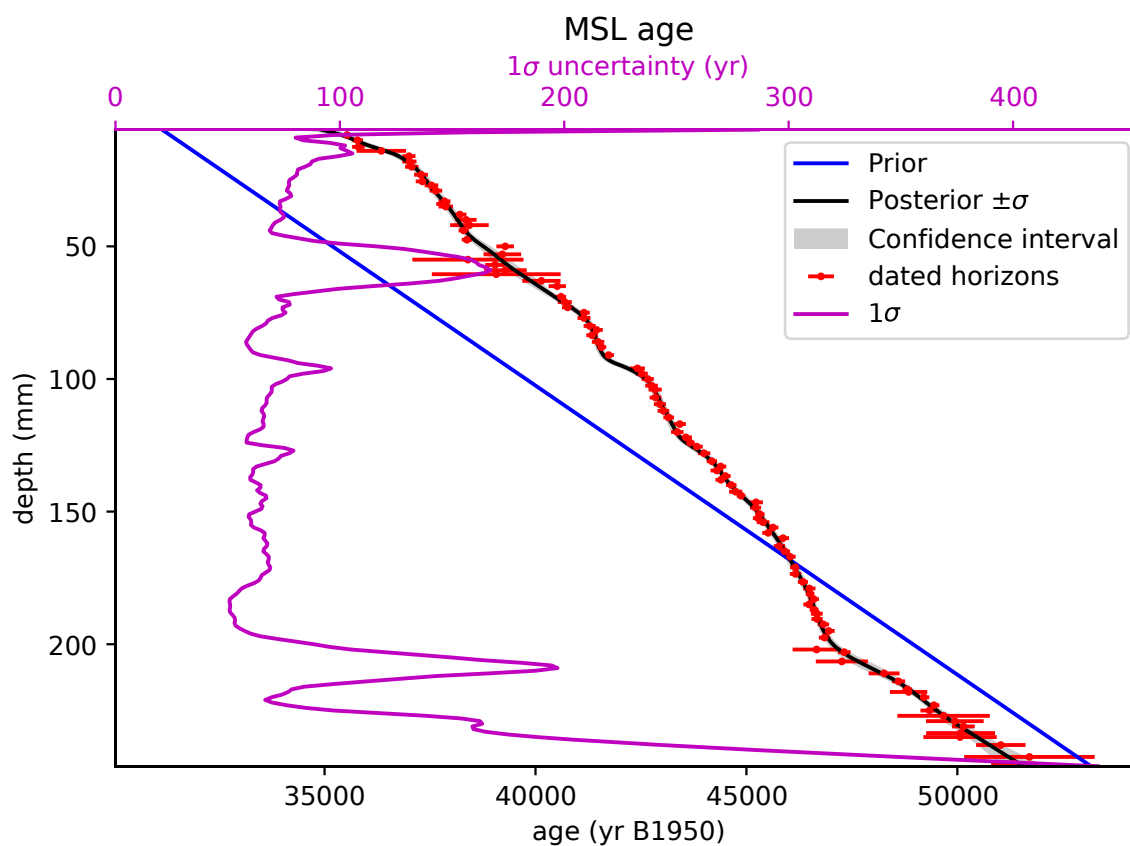
Figure 3: Age graph for the MSL speleothem as produced by Paleochrono-1.1 in the AICC2023-Hulu dating experiment. Blue: prior chronology based on the sedimentation scenario. Black and grey: posterior chronology and its confidence interval after optimization by Paleochrono-1.1. Red: dated horizons used in the dating experiment. Pink: 1sigma uncertainty of the posterior chronology.
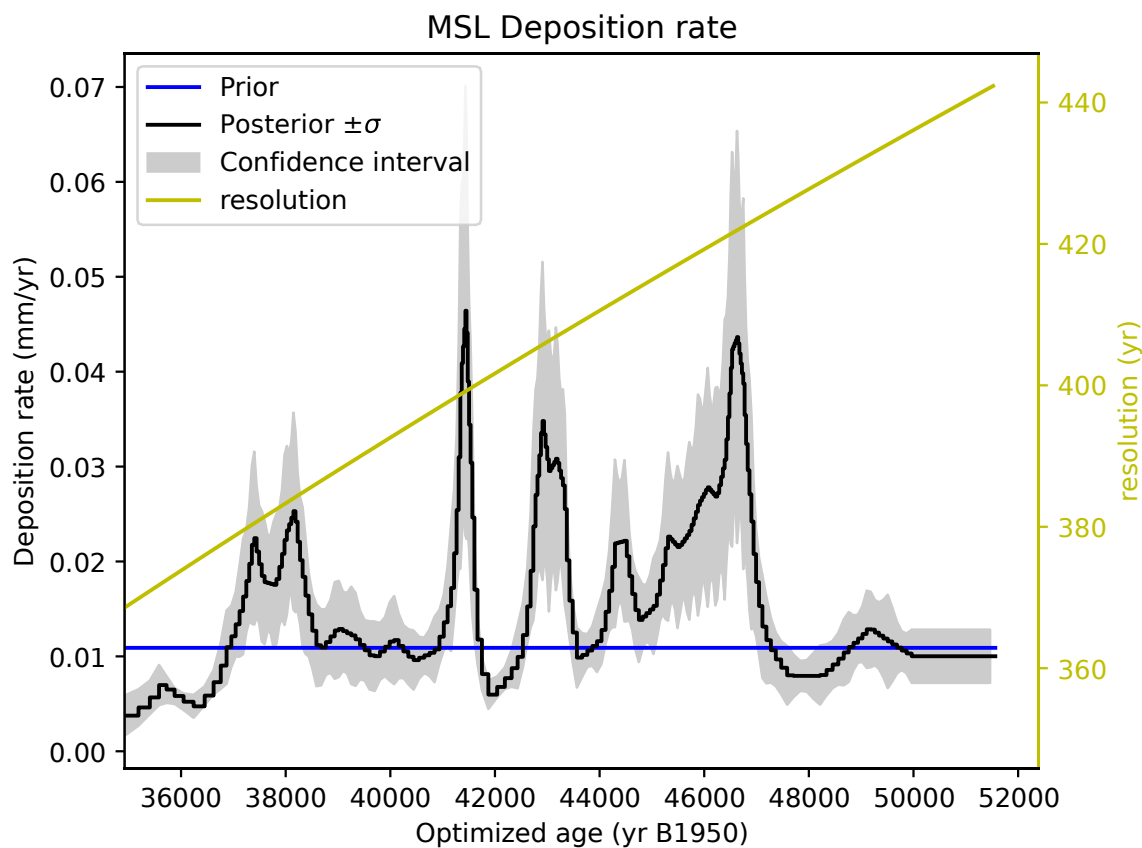
Figure 4: Deposition/growth rate graph for the MSL speleothem as produced by Paleochrono-1.1 in the AICC2023-Hulu dating experiment. Blue: prior scenario. Black and grey: posterior scenario and its confidence interval after optimization by Paleochrono-1.1. Yellow: time resolution of the deposition rate in the inversion grid.
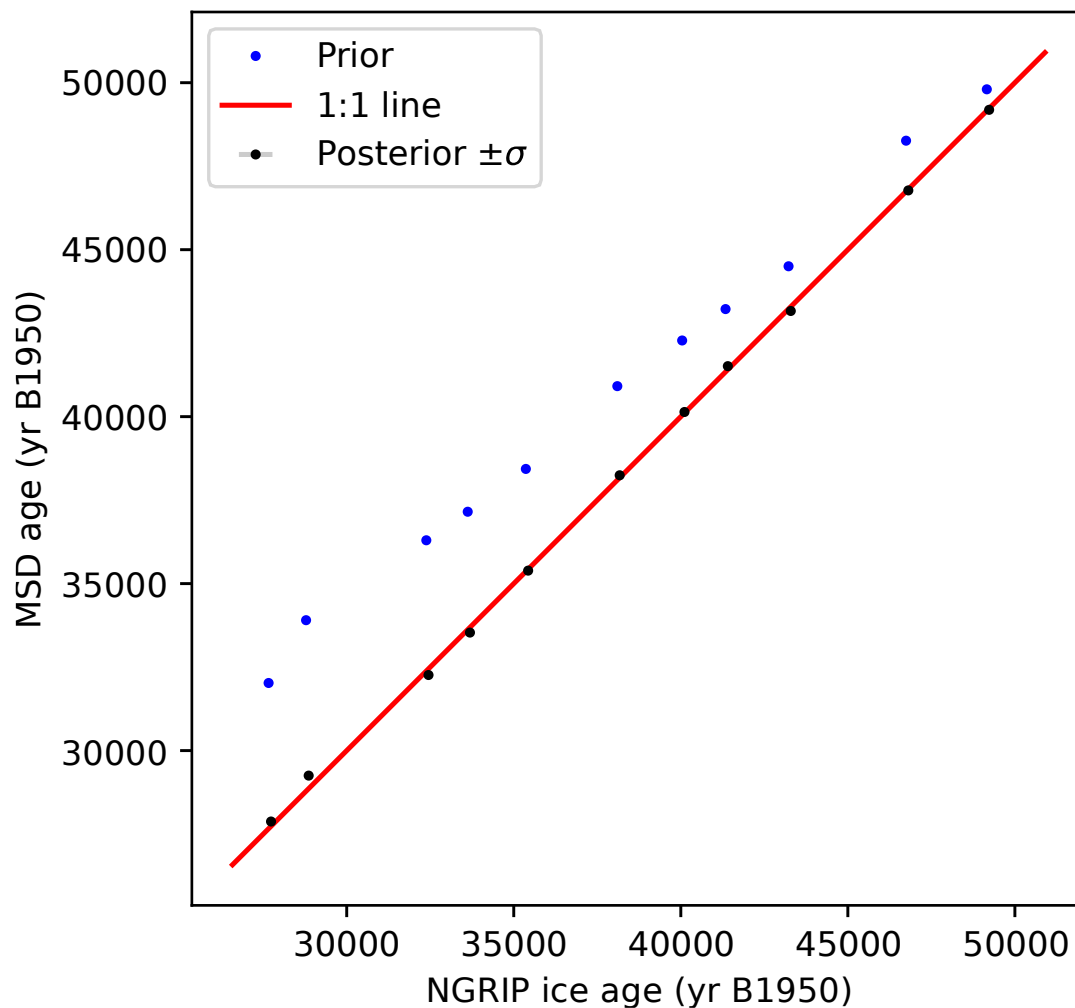
Figure 5: Synchronisation graph for the NGRIP-MSD site pair as produced by Paleochrono-1.1 in the AICC2023-Hulu dating experiment. Blue: prior scenario. Black: posterior scenario after optimization by Paleochrono-1.1. Red: the 1:1 line for comparison.
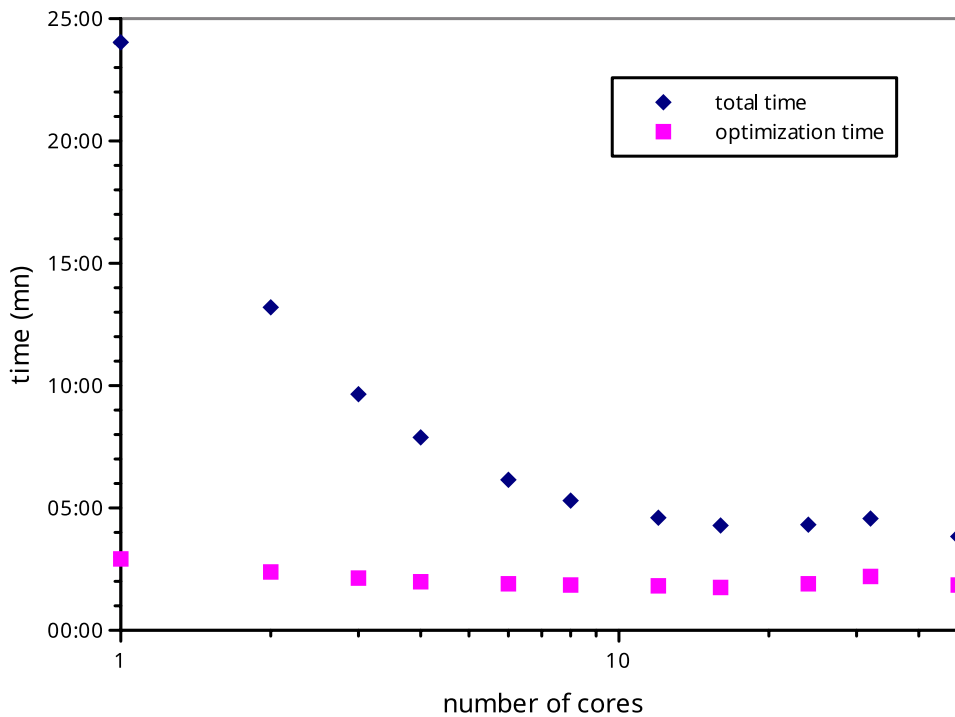
Figure 6: Computing time of the AICC2023 dating experiment using Paleochrono-1.1, as a function of the number of computing cores.
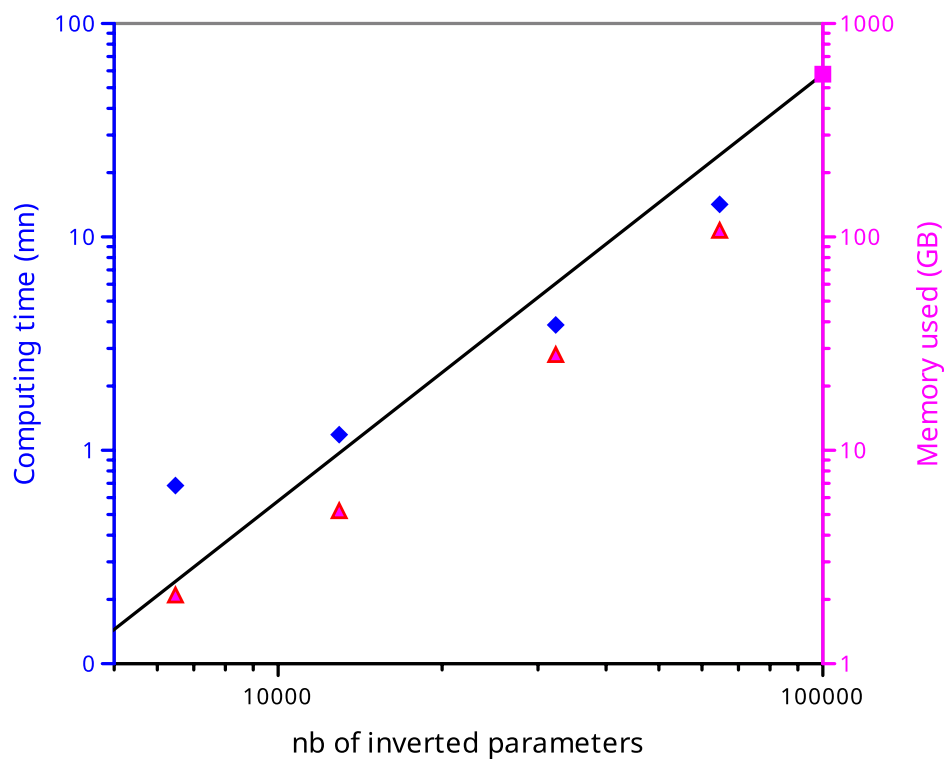
Figure 7: Computing time and memory used by Paleochrono-1.1 in the AICC2023 dating experiment, as a function of the number of inverted parameters. The X- and Y-axes are logarithmic. The black line represent a quadratic evolution of the resources with respect to the number of parameters.

730